Journal of Biomechanics 47 (2014) 750–754

Contents lists available at ScienceDirect

Journal of Biomechanics

journal homepage: www.elsevier.com/locate/jbiomech
www.JBiomech.com

Short communication

The use of 2D ultrasound elastography for measuring tendon motion and strain

Laura Chernak Slane [a,*], Darryl G. Thelen [a,b,c]

[a] Department of Biomedical Engineering, 1513 University Ave, University of Wisconsin-Madison, WI 53705, USA
[b] Department of Mechanical Engineering, University of Wisconsin-Madison, WI, USA
[c] Department of Orthopedics and Rehabilitation, University of Wisconsin-Madison, WI, USA

ARTICLE INFO

Article history:
Accepted 18 November 2013

Keywords:
Tendon mechanics
Ultrasound elastography

ABSTRACT

The goal of the current study was to investigate the fidelity of a 2D ultrasound elastography method for the measurement of tendon motion and strain. Ultrasound phantoms and *ex vivo* porcine flexor tendons were cyclically stretched to 4% strain while cine ultrasound radiofrequency (RF) data and video data were simultaneously collected. 2D ultrasound elastography was used to estimate tissue motion and strain from RF data, and surface tissue motion and strain were separately estimated using digital image correlation (DIC). There were strong correlations ($R^2 > 0.97$) between DIC and RF measurements of phantom displacement and strain, and good agreement in estimates of peak phantom strain (DIC: $3.5 \pm 0.2\%$; RF: $3.7 \pm 0.1\%$). For tendon, elastographic estimates of displacement profiles also correlated well with DIC measurements ($R^2 > 0.92$), and exhibited similar estimated peak tendon strain (DIC: $2.6 \pm 1.4\%$; RF: $2.2 \pm 1.3\%$). Elastographic tracking with B-Mode images tended to under-predict peak strain for both the phantom and tendon. This study demonstrates the capacity to use quantitative elastographic techniques to measure tendon displacement and strain within an ultrasound image window. The approach may be extendible to in vivo use on humans, which would allow for the non-invasive analysis of tendon deformation in both normal and pathological states.

1. Introduction

Quantitative ultrasound imaging techniques have emerged for characterizing in vivo tendon motion and deformation. The most common approach involves manually tracking the relative motion of a muscle-tendon junction across cine B-Mode images, and then using that information to compute average tissue strain (Maganaris and Paul, 1999, 2002; Magnusson et al., 2001; Peixinho et al., 2008). When coupled with force measurements, such methods have been used to assess the effects of training (Maganaris, 2003) and aging (Karamanidis and Arampatzis, 2005) on tendon elasticity. More recent work has shown progress in developing automated methods for tracking motion of the muscle-tendon junction (Gerus et al., 2011; Stenroth et al., 2012) and free tendon (Arndt et al., 2012). Although there is mounting evidence that micro tendon deformations are nonuniform (Cheng and Screen, 2007; Arndt et al., 2012) and dependent on fiber organization (Thorpe et al., 2013a, 2013b), it remains challenging to track spatial variations in tendon deformation with ultrasound. Thus, it would be advantageous if tendon displacement and strain patterns could be assessed within an ultrasound image window to provide more localized measures of tissue deformation.

Ultrasound elastography is an approach that uses correlation based tracking of successive ultrasound images to estimate tissue deformation (Ophir et al., 1991), with the phase information in ultrasound radiofrequency (RF) data enabling high resolution tracking of tissue motion along the beam direction (Bohs and Trahey, 1991; Lopata et al., 2009; Ophir et al., 1999). Although tissue deformation in elastography is often achieved via manual compression (De Zordo et al., 2010; De Zordo et al., 2009), we have been interested in adapting elastography principles to track tendon deformation under loading conditions that are more physiologically relevant (Chernak and Thelen, 2012). Adapting elastography for tracking tendon can be challenging due to a variety of factors, including the lower resolution of ultrasound data in a direction transverse to the sound beam (Ophir et al., 1999) and the complex architectural features of tendon. Recent advances in 2D elastographic tracking methods have emerged (Chen et al., 2004; Ebbini, 2006; Huang and O'Donnell, 2010) that may be capable of addressing these challenges. The purpose of this study, therefore, was to investigate the fidelity of a 2D elastography method for evaluating motion and strain of tendon-shaped phantoms and *ex vivo* tendon specimens subjected to axial loading. Motion and strain data from elastography were compared

* Corresponding author. Tel.: +1 608 603 6692; fax: +1 608 265 2316.
E-mail address: laura.a.slane@gmail.com (L. Chernak Slane).

0021-9290/$ - see front matter © 2013 Elsevier Ltd. All rights reserved.
http://dx.doi.org/10.1016/j.jbiomech.2013.11.023

with surface motion and strain measures obtained using digital image correlation (DIC) (Sutton et al., 1983). We also compared elastographic estimates obtained with RF and B-Mode data to better understand the potential advantages of using RF data to enhance tissue tracking.

2. Methods

Tendon-shaped phantom specimens and *ex vivo* porcine flexor tendons were tested using an identical protocol (Fig. 1). Phantoms ($12.7 \times 14.3 \times 101.6\ mm^3$) were created from polyvinyl chloride-plastisol (Spirou et al., 2005) with randomly dispersed glass beads (30–50 μm diameter) used as ultrasound scatter particles (Insana et al., 1990). Porcine flexor tendons were dissected with the distal bone intact, wrapped in a saline-soaked gauze pad, and frozen until one hour prior to testing. An oil-based paint speckle pattern was applied to each specimen surface to enable DIC tracking. The specimens were submerged in a saline solution bath (9 g NaCL/L of water), with the ends fixed in custom grips (Cheung and Zhang, 2006) of a materials testing machine (Criterion 43, MTS Systems Corporation, Eden Prairie, MN). Specimens were preconditioned with cyclic stretch (0.5 Hz) to 2% strain for ten cycles, followed by three trials of cyclic loading (0.5 Hz) to 4% strain for ten cycles. Prior to each test, specimens were given seven minutes of rest, preloaded to 10 N, and the grip-to-grip length (mean: 84.6 ± 2.9 mm) was measured.

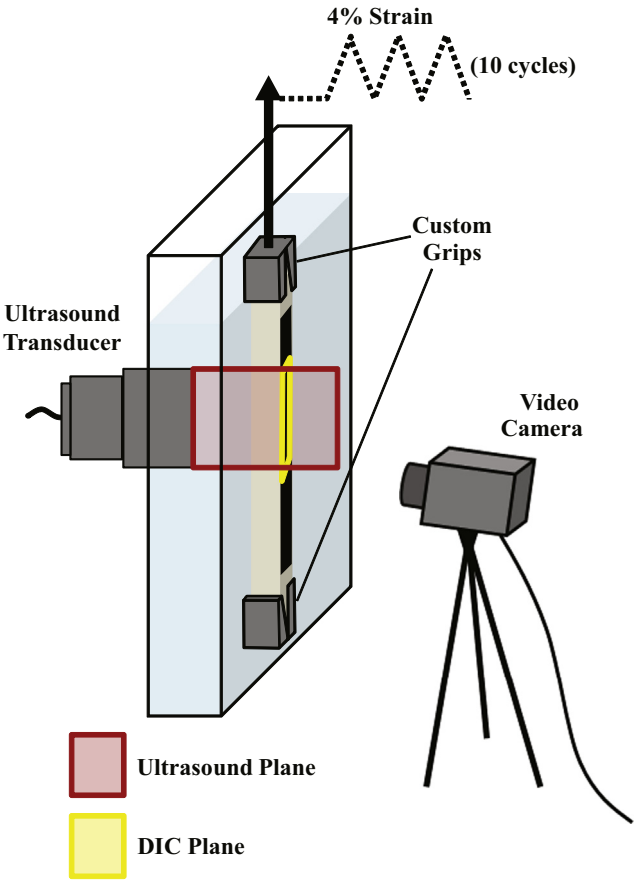

Fig. 1. Overview of data collection methods. The specimen is mounted in custom grips and cyclically stretched to 4% strain. The ultrasound transducer is positioned to collect cine RF data from a fixed longitudinal cross-section of the specimen. A video camera was positioned to simultaneously collect surface images of the same tendon region.

A linear array ultrasound transducer (L14-5/38, Ultrasonix Corporation, Richmond, BC, Canada) was positioned to collect RF data in a fixed image plane ($35 \times 38\ mm^2$, 128×1824 pixels, 56 frames/sec). Video images (2048×2448 pixels, Vic-Snap, Correlated Solutions, Inc., Columbia, SC) were collected simultaneously such that the specimen and transducer were in view. For DIC analysis, a region of interest (ROI; Phantom: $\sim 38 \times 12\ mm^2$; Tendon: $38 \times \sim 4$ mm) was manually defined to align with the center of the transducer from an unstretched frame of data. Data were tracked (Vic-2D Version 2009, Correlated Solutions, Inc., Columbia, SC) using a seed point defined near the stationary grip (Vic-2D parameters, subset: 40, step size: 5), with the results used to compute strains. For each trial, we reviewed the DIC tracking results, load cell information and ultrasound images to ensure that out-of-plane motion was small, there was no evidence of slip and tendon fascicles remained in view throughout loading. All three phantoms and eight of the twelve porcine flexor tendons achieved these criteria and were included in the subsequent analysis.

Ultrasound data were evaluated using a custom 2D elastography method that has been described previously (Chernak and Thelen, 2012). Briefly, the RF data were upsampled by a factor of 2 and 4 in the along-fiber (x) and transverse (y) directions (Parker et al., 1983) to increase the spatial density of correlation functions (Konofagou and Ophir, 1998). An ROI was defined within the specimen (Phantom: $\sim 28.3 \times 7.7\ mm^2$; Tendon: $\sim 26.1 \times 3.9\ mm^2$). Kernels ($2 \times 0.8\ mm^2$) were centered at nodes positioned every 1.0 and 0.4 mm along the x and y directions, respectively (Fig. 2). The peak of a 2D normalized cross-correlation function was used to estimate frame-to-frame (incremental) kernel displacements. Sub-pixel displacements were defined as the maximum of a quartic surface spline fit of the correlations (Azar et al., 2010). Incremental displacements (du, dv) were median filtered (3×3 nodes) (Thitaikumar et al., 2008), and fitted with low-order polynomials to regularize the displacements (Pan et al., 2009). The along-fiber incremental displacements, du, were assumed to vary as a quadratic function of the nodal positions, x and y:

$$du = A_1x^2 + A_2y^2 + A_3xy + A_4x + A_5y + A_6$$

The higher resolution along-beam incremental displacements, dv, were assumed to vary quadratically along each row of nodes at a fixed initial x position along the specimen:

$$dv = B_1y^2 + B_2y + B_3$$

Polynomial parameters A_i and B_i were computed using a least squares fit to the experimental data. Nodal displacements, u and v, were updated at each frame by adding on the incremental displacements. Nodal tracking was repeated in the reverse direction and a weighted average of the nodal displacement trajectories from the forward and backward tracking results was computed (Pelc, 1995). Along-fiber strain $e_{x,i}$, at a node i, was estimated using a small strain assumption between nodes along the fascicles:

$$e_{x,i} = \frac{u_{i+1} - u_{i-1}}{x_{0,i+1} - x_{0,i-1}}$$

where x_0 represent the nodal positions in a relaxed frame, u represent nodal translations in the x direction and $i+1$ and $i-1$ refer to nodes to either side of the node of interest. Elastographic analysis was repeated on B-Mode image data

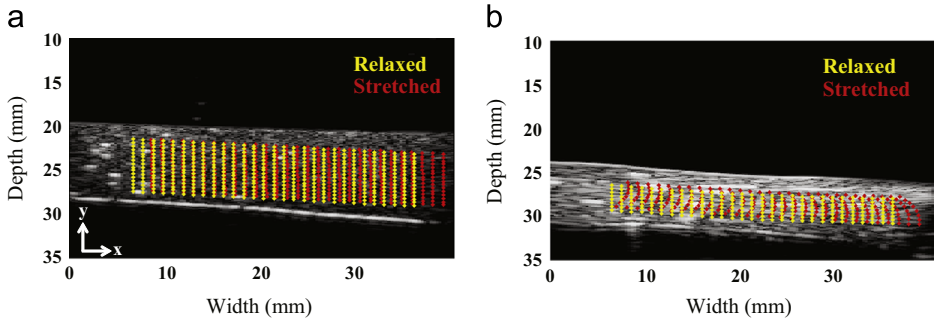

Fig. 2. Nodal positions during relaxed and stretched frames of a sample phantom and tendon specimen. As this example shows, the phantoms tended to undergo more uniform deformation than the tendon. (a) Phantom and (b) Tendon.

generated from the RF data using a log compression and the Hilbert transform:

$$B-Mode = 20\log_{10}(abs(Hilbert(RF)))$$

We quantitatively compared the displacements and strains obtained using DIC and elastographic analyses by computing the correlation between trajectories over a loading cycle. We also performed paired t-tests to assess differences in estimates of peak strains between methods.

3. Results

3.1. Phantom tracking

There was very good agreement ($R^2 > 0.97$) between DIC and RF elastographic estimates of phantom displacement (Fig. 3a) and strain (Fig. 4a) trajectories (Table 1). Peak phantom strain (DIC: $e_x = 3.5 \pm 0.2\%$; RF: $e_x = 3.7 \pm 0.1\%$) was also comparable between methods (Fig. 4a). However, elastographic tracking with B-Mode images resulted in an under-prediction of motion (Fig. 3a) and significant ($p < 0.05$) under-prediction ($1.9 \pm 0.8\%$) of peak strain.

3.2. Tendon tracking

The tendon displacement trajectories computed with RF elastography were highly correlated with the DIC measurements ($R^2 > 0.92$; Fig. 3b). Both the DIC and elastographic strain estimates exhibited nonlinear strain-stiffening behavior with loading, with reasonably strong correlations ($R^2 = 0.77$; Fig. 4b) and comparable estimates of peak tendon strain (DIC: $e_x = 2.6 \pm 1.4\%$; RF: $e_x = 2.2 \pm 1.3\%$). Elastographic tendon strain computed with B-Mode images tended to be lower ($e_x = 1.5 \pm 1.0\%$) than those obtained with DIC and RF data.

4. Discussion

This study demonstrates that 2D elastography methods can produce reasonably accurate displacement and strain estimates arising from axial loading of tendon. The notable benefit of this technique is that all analysis is based on data contained within the transducer image window, which obviates the need for using multiple transducers or pre-assuming motion that is out of view. Furthermore, images of spatial variations in tissue motion (Fig. 2) may provide new insights into the complex deformation patterns of functionally loaded tendon (Arndt et al., 2012; Finni et al., 2003; Magnusson et al., 2003; Muramatsu et al., 2001).

Two-dimensional elastographic tracking (Chen et al., 2004; Ebbini, 2006; Huang and O'Donnell, 2010; Lubinski et al., 1999) remains challenging due to limitations in lateral resolution and the potential for out-of-plane motion to obscure 2D displacement estimates. In this *ex vivo* study, we were able to visually ensure that an imaging plane could be defined that aligned with the primary plane of motion. Extending the approach to in vivo studies will require better understanding of the sensitivity of

Table 1
The average (± 1 sd) correlation (Pearson's R^2) between DIC and elastographic estimates of displacement and strain trajectories. Elastographic tracking of tendon deformation was highly correlated with DIC measures when using either the RF or B-Mode (BM) ultrasound data. However in the tendons, elastographic tracking with RF data produced trajectories that were more consistent with DIC estimates than B-Mode based tracking.

		Phantom	Tendon
Disp.	RF	0.992 ± 0.006	0.975 ± 0.027
	BM	0.976 ± 0.019	0.921 ± 0.161
Strain	RF	0.992 ± 0.001	0.765 ± 0.262
	BM	0.972 ± 0.014	0.634 ± 0.307

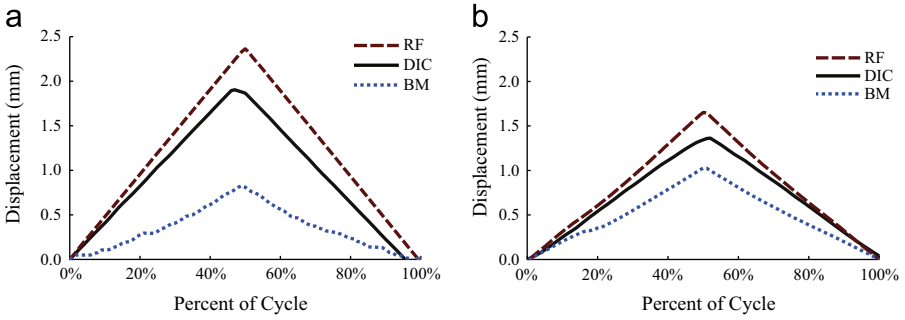

Fig. 3. Sample displacement trajectories estimated using digital image correlation (DIC) analysis of the video data and 2D elastographic analysis of ultrasound data (RF). Elastographic tracking using B-Mode (BM) images tended to under-estimate motion, as was most evident in the phantom specimens. (a) Phantom and (b) Tendon.

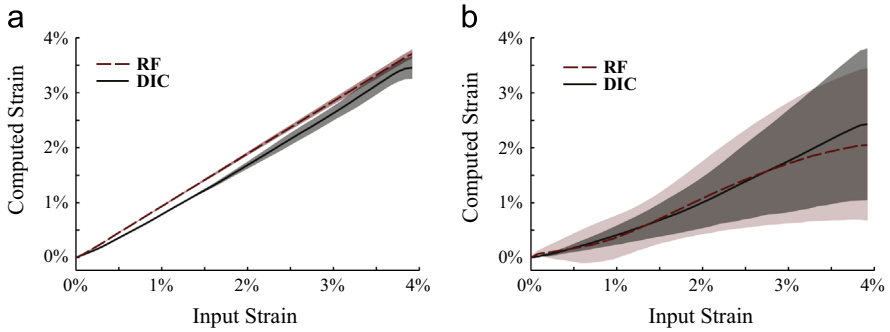

Fig. 4. Average (shaded curve is $\pm$ sd) DIC and RF strain trajectories with loading for both the phantom and tendon specimens. Mid-substance strains were less than the grip-to-grip strain (plotted along the x-axis), with larger differences observed in the tendon specimens. (a) Phantom and (b) Tendon.

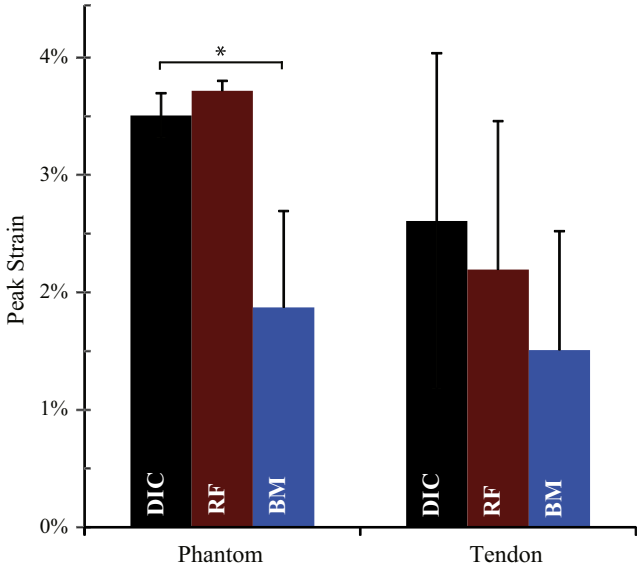

Fig. 5. The average (+ 1 sd) peak strain estimates obtained using DIC and elastographic analysis of RF and B-Mode (BM) image data. Average mid-substance phantom strains were significantly less than the strains computed using DIC analysis of video data (*$p < 0.05$).

tissue displacement estimates to variations in tendon orientation. To address resolution issues, we used quartic spline fits of the correlation function to obtain sub-pixel motion estimates (Azar et al., 2010) and low-order polynomial fits to regularize displacement and strain estimates (Pan et al., 2009). We note that this regularization approach does diminish one's ability to resolve subtle variations in tissue deformation. Thus, it will be important to consider more sophisticated regularization approaches when using the elastographic approach for assessing motion in tendons with localized damage.

Our results suggest that tracking is enhanced using RF data rather than B-Mode images. Elastographic analysis of B-Mode data tended to result in an under-prediction of motion and strain in both the phantom and flexor tendons (Fig. 5). Although prior studies have used RF data to assess tendon deformation with compression (Brown et al., 2013; Korstanje et al., 2009; Korstanje et al., 2010), we believe this is the first study to demonstrate the benefit of using RF signals to track tendon motion under axial loading. The difference in tracking accuracy is likely attributable to the greater precision achieved by using the phase information inherent in RF data to track fine displacements (Lopata et al., 2009). We note that B-Mode images were generating using a simple Hilbert transformation, which may not reflect the B-Mode processing methods of commercial ultrasound systems.

Both the DIC and elastography methods in this study consistently predicted maximum mid-substance tendon strains that were less than the grip-to-grip strain. This phenomenon is well-documented in the literature (Haraldsson et al., 2005), and is likely due to higher strains arising near the site of tissue clamping. Although the test setup (Fig. 1) allowed us to directly compare displacements and strains of the same region of the specimen for both methods, it is important to note the different imaging planes of the surface DIC measures and the ultrasound cross-sectional information. This difference could have contributed to some of the variability in motion and strain between methods (Figs. 3–5).

In summary, this study demonstrates the fidelity of a 2D elastography tracking method for measuring displacement and strain using ultrasound RF data collected during axial tendon loading. The approach may be extendible to in vivo use on humans, which would allow for quantitative analysis of tendon deformation in both normal and pathological states.

Conflict of interest statement

The authors have no conflict of interest.

Acknowledgments

NIH F31AG043216, International Society of Biomechanics Matching Dissertation Fund, Daniel Volk, Alex Ehlers.

References

Arndt, A., Bengtsson, A.S., Peolsson, M., Thorstensson, A., Movin, T., 2012. Non-uniform displacement within the Achilles tendon during passive ankle joint motion. Knee Surg., Sports Traumatol., Arthrosc.: Off. J. Eur. Soc. Sports Traumatol., Knee Surg. Arthrosc. 20, 1868–1874.

Azar, R.Z., Goksel, O., Salcudean, S.E., 2010. Sub-sample displacement estimation from digitized ultrasound rf signals using multi-dimensional polynomial fitting of the cross-correlation function. IEEE. Trans. Ultrason. Ferroelectr. Freq. Control. 57, 2403–2420.

Bohs, L.N., Trahey, G.E., 1991. A novel method for angle independent ultrasonic-imaging of blood-flow and tissue motion. IEEE Trans. Biomed. Eng. 38, 280–286.

Brown, P.G., Alsousou, J., Cooper, A., Thompson, M.S., Noble, J.A., 2013. The AutoQual ultrasound elastography method for quantitative assessment of lateral strain in post-rupture Achilles tendons. J. Biomech. 46, 2695–2700.

Chen, X.C., Zohdy, M.J., Emelianov, S.Y., O'Donnell, M., 2004. Lateral speckle tracking using synthetic lateral phase. IEEE Trans. Ultrason., Ferroelectrics Freq. Control 51, 540–550.

Cheng, V.W.T., Screen, H.R.C., 2007. The micro-structural strain response of tendon. J. Mater. Sci. 42, 8957–8965.

Chernak, L.A., Thelen, D.G., 2012. Tendon motion and strain patterns evaluated with two-dimensional ultrasound elastography. J. Biomech. 45, 2618–2623.

Cheung, J.T., Zhang, M., 2006. A serrated jaw clamp for tendon gripping. Med. Eng. Phys. 28, 379–382.

De Zordo, T., Chhem, R., Smekal, V., Feuchtner, G., Reindl, M., Fink, C., Faschingbauer, R., Jaschke, W., Klauser, A.S., 2010. Real-time sonoelastography: findings in patients with symptomatic achilles tendons and comparison to healthy volunteers. Ultraschall in der Medizin 31, 394–400.

De Zordo, T., Lill, S.R., Fink, C., Feuchtner, G.M., Jaschke, W., Bellmann-Weiler, R., Klauser, A.S., 2009. Real-time sonoelastography of lateral epicondylitis: comparison of findings between patients and healthy volunteers. Am. J. Roentgenol. 193, 180–185.

Ebbini, E.S., 2006. Phase-coupled two-dimensional speckle tracking algorithm. IEEE Trans. Ultrason., Ferroelectr. Freq. Control 53, 972–990.

Finni, T., Hodgson, J.A., Lai, A.M., Edgerton, V.R., Sinha, S., 2003. Mapping of movement in the isometrically contracting human soleus muscle reveals details of its structural and functional complexity. J. Appl. Physiol. 95, 2128–2133.

Gerus, P., Rao, G., Berton, E., 2011. A method to characterize in vivo tendon force-strain relationship by combining ultrasonography, motion capture and loading rate. J. Biomech. 44, 2333–2336.

Haraldsson, B.T., Aagaard, P., Krogsgaard, M., Alkjaer, T., Kjaer, M., Magnusson, S.P., 2005. Region-specific mechanical properties of the human patella tendon. J. Appl. Physiol. 98, 1006–1012.

Huang, L., O'Donnell, M., 2010 A synthetic lateral phase (SLP) displacement estimator using complex FIR filters. In: Proceedings of the Ultrasonics Symposium (IUS), 2010 IEEE.

Insana, M.F., Wagner, R.F., Brown, D.G., Hall, T.J., 1990. Describing small-scale structure in random-media using pulse-echo ultrasound. J. Acoust. Soc. Am. 87, 179–192.

Karamanidis, K., Arampatzis, A., 2005. Mechanical and morphological properties of different muscle-tendon units in the lower extremity and running mechanics: effect of aging and physical activity. J. Exp. Biol. 208, 3907–3923.

Konofagou, E., Ophir, J., 1998. A new elastographic method for estimation and imaging of lateral displacements, lateral strains, corrected axial strains and Poisson's ratios in tissues. Ultrasound Med. Biol. 24, 1183–1199.

Korstanje, J., Selles, R., Henk, S., Hovius, S., Bosch, J., 2009. Dedicated ultrasound speckle tracking to study tendon displacement. In: Proceedings of the Conference SPIE Medical Imaging 2009: Ultrasonic Imaging and Signal Processing. Lake Buena Vista, FL, USA.

Korstanje, J.W., Selles, R.W., Stam, H.J., Hovius, S.E., Bosch, J.G., 2010. Development and validation of ultrasound speckle tracking to quantify tendon displacement. J. Biomech 43, 1373–1379.

Lopata, R.G.P., Nillesen, M.M., Hansen, H.H.G., Gerrits, I.H., Thijssen, J.M., de Korte, C. L., 2009. Performance evaluation of methods for two-dimensional displacement and strain estimation using ultrasound radio frequency data. Ultrasound Med. Biol. 35, 796–812.

Lubinski, M.A., Emelianov, S.Y., O'Donnell, M., 1999. Speckle tracking methods for ultrasonic elasticity imaging using short-time correlation. IEEE. Trans. Ultrason. Ferroelectr. Freq. Control. 46, 82–96.
Maganaris, C.N., 2003. Tendon conditioning: artefact or property? Proc. R. Soc. – Biol. Sci. 270 (Suppl 1), S39–42.
Maganaris, C.N., Paul, J.P., 1999. In vivo human tendon mechanical properties. J. Physiol. 521 (Pt 1), 307–313.
Maganaris, C.N., Paul, J.P., 2002. Tensile properties of the in vivo human gastrocnemius tendon. J. Biomech. 35, 1639–1646.
Magnusson, S.P., Aagaard, P., Dyhre-Poulsen, P., Kjaer, M., 2001. Load–displacement properties of the human triceps surae aponeurosis in vivo. J. Physiol. 531, 277–288.
Magnusson, S.P., Hansen, P., Aagaard, P., Brond, J., Dyhre-Poulsen, P., Bojsen-Moller, J., Kjaer, M., 2003. Differential strain patterns of the human gastrocnemius aponeurosis and free tendon, in vivo. Acta. Physiol. Scand. 177, 185–195.
Muramatsu, T., Muraoka, T., Takeshita, D., Kawakami, Y., Hirano, Y., Fukunaga, T., 2001. Mechanical properties of tendon and aponeurosis of human gastrocnemius muscle in vivo. J. Appl. Physiol. 90, 1671–1678.
Ophir, J., Alam, S.K., Garra, B., Kallel, F., Konofagou, E., Krouskop, T., Varghese, T., 1999. Elastography: ultrasonic estimation and imaging of the elastic properties of tissues. Proc. Inst. Mech. Eng. Part H, J. Eng. Med. 213, 203–233.
Ophir, J., Céspedes, I., Ponnekanti, H., Yazdi, Y., Li, X., 1991. Elastography: a quantitative method for imaging the elasticity of biological tissues. Ultrason. Imaging. 13, 111–134.
Pan, B., Qian, K., Xie, H., Asundi, A., 2009. Two-dimensional digital image correlation for in-plane displacement and strain measurement: a review. Meas. Sci. Technol., 20.
Parker, J., Kenyon, R.V., Troxel, D.E., 1983. Comparison of interpolating methods for image resampling. IEEE. Trans. Med. Imaging. 2, 31–39.
Peixinho, C.C., Alves, D.S., Lacerda, R.G., Vieira, T.M.M., Oliveira, L.F., 2008. Strain and slackness of achilles tendon during passive joint mobilization via imaging ultrasonography. Revista Brasileira de Fisioterapia 12, 366–372.
Pelc, N.J., 1995. Flow quantification and analysis methods. Magn. Reson. Imaging Clin. N. Am. 3, 413–424.
Spirou, G.M., Oraevsky, A.A., Vitkin, I.A., Whelan, W.M., 2005. Optical and acoustic properties at 1064 nm of polyvinyl chloride-plastisol for use as a tissue phantom in biomedical optoacoustics. Phys. Med. Biol. 50, N141–N153.
Stenroth, L., Peltonen, J., Cronin, N.J., Sipila, S., Finni, T., 2012. Age-related differences in Achilles tendon properties and triceps surae muscle architecture in vivo. J. Appl. Physiol. 113, 1537–1544.
Sutton, M.A., Wolters, W.J., Peters, W.H., Ranson, W.F., McNeill, S.R., 1983. Determination of displacements using an improved digital correlation method. Image Vision Comput. 1, 133–139.
Thitaikumar, A., Mobbs, L.M., Kraemer-Chant, C.M., Garra, B.S., Ophir, J., 2008. Breast tumor classification using axial shear strain elastography: a feasibility study. Phys. Med. Biol. 53, 4809–4823.
Thorpe, C.T., Udeze, C.P, Birch, H.L., Clegg, P.D., Screen, H.R., 2013a. Capacity for sliding between tendon fascicles decreases with ageing in injury prone equine tendons: a possible mechanism for age-related tendinopathy? Eur. Cells Mater. 24, 48–60.
Thorpe, C.T., Klemt, C., Riley, G.P., Birch, H.L., Clegg, P.D., Screen, H.R., 2013b. Helical sub-structures in energy-storing tendons provide a possible mechanism for efficient energy storage and return. Acta. Biomater. 9, 7948–7956.